Health and Technology (2023) 13:101–110
https://doi.org/10.1007/s12553-022-00718-y

ORIGINAL PAPER

SPECT/CT-based dosimetry of salivary glands and iodine-avid lesions following ^{131}I therapy

Mohammad Abuqbeitah[1] · Mustafa Demir[1] · Sağit Sağer[1] · Sertaç Asa[1] · Nazenin Ipek Işıkcı[2] · Kerim Sönmezoğlu[1]

Received: 10 September 2022 / Accepted: 19 December 2022 / Published online: 6 January 2023

Abstract

Objective The purpose was to provide uptake and radiation dose estimates to salivary glands (SG) and pathologic lesions following radioiodine therapy (RIT) of differentiated thyroid cancer patients (DTC).

Methods A group of DTC patients (n = 25) undergoing ^{131}I therapy joined this study with varying amounts of therapeutic activity. Sequential SPECT/CT scans were acquired at 4 ± 2, 24 ± 2, and 168 ± 3 h following administration of 3497–9250 MBq 131I. An earlier experiment with Acrylic glass body phantom (PET Phantom NEMA 2012 / IEC 2008) was conducted for system calibration including scatter, partial volume effect and count loss correction. Dose calculation was made via IDAC-Dose 2.1 code.

Results The absorbed dose to parotid glands was 0.04–0.97 Gy/GBq (median: 0.26 Gy/GBq). The median absorbed dose to submandibular glands was 0.14 Gy/GBq (0.05 to 0.56 Gy/GBq). The absorbed dose to thyroid residues was from 0.55 to 399.5 Gy/GBq (median: 21.8 Gy/GBq), and that to distal lesions ranged from 0.78 to 28.0 Gy/GBq (median: 3.12 Gy/GBq). 41% of the thyroid residues received dose > 80 Gy, 18% between 70–80 Gy, 18% between 40–70 Gy, and 23% has dose < 40 Gy. In contrast, 18% of the metastases exhibited a dose > 80 Gy, 9% between 40–60 Gy, and the dose to the vast majority of lesions (64%) was < 40 Gy.

Conclusion It was inferred that dose estimation after RIT with SPECT/CT is feasible to apply, together with good agreement with published ^{124}I PET/CT dose estimates. A broad and sub-effective dose range was estimated for thyroid residues and distal lesions. Moreover, the current methodology might be useful for establishing a dose–effect relationship and radiation-induced salivary glands damage after RIT.

Keywords Salivary glands · ^{131}I therapy · Thyroid remnants · Absorbed dose · SPECT/CT

1 Introduction

Thyroid cancer has been shown responsible for 0.2—0.5% of cancer-related deaths. In particular, well-differentiated thyroid cancer (DTC) is considered the most common type making up around 85–95% of all thyroid cancers [1, 2]. In DTC management, total thyroidectomy is deemed the curative-intent therapy of DTC followed by adjuvant radioiodine therapy (RIT) to eradicate occult microscopic thyroid foci, extra-thyroidal extensions, involvement of lymph nodes, and distant metastases [3]. ^{131}I is a β- emitting radionuclide that decays to stable xenon-131 with a physical half-life of 8.02 days, a principal γ-ray of 364 keV, maximum β- energy of 0.61 MeV, and linear energy transfer of 0.25 keV/μm [4]. The therapeutic activity is often a standardized activity chosen empirically with less focus on personalized dosimetry. After oral administration, radioiodine systemically circulates through the entire body with mounting uptake in thyroid residues and iodine avid lesion. In the meantime, well-perfused organs such as red marrow and kidneys are exposed to the risk of radiation-induced malfunctions [5, 6].

Furthermore, the main salivary glands (parotid, submandibular, and sublingual) secret about 90% of the saliva in the oral cavity, while only 5% is released from minor lingual glands [7]. In RIT, salivary glands concentrate radioiodine 7–700 times the serum level due to overexpression of sodium/iodide symporter (NIS). This status leads to the most prevalent side effect (sialadenitis) occurring in 10–60% of the treated patients with RI in addition to sensation of a dry mouth (xerostomia), and an increased risk of oral infections and dental caries [8–12]. It was also found that 20% of salivary glands became dysfunctional

✉ Mohammad Abuqbeitah
qbeta95@hotmail.com

[1] Cerrahpasa Faculty of Medicine, Department of Nuclear Medicine, Istanbul University - Cerrahpasa, Istanbul, Turkey

[2] Faculty of Engineering and Architecture, Department of Genetics and Bioengineering, Nisantasi University, Istanbul, Turkey

after 5 years of a single ^{131}I dose and exposure to about 45 Gy may cause significant damage to salivary glands [13–15]. So far, lemon sucking and chewing gum are routinely used to reduce the iodine residence in salivary glands. More recently, phenylephrine has been shown effective to alleviate ^{131}I radiation damage by maintaining mitochondrial homeostasis [16].

On the other hand, the finite resolution of the nuclear imaging systems constituted an obstacle to providing exemplary dose calculation to lesions. Thus, the trend was directed to administer maximum permissible activity limited by the dose boundaries of the organs at risk (e.g. red marrow in RIT) [17]. Presently, lesions detection and physical modeling of the image have been improved with the advent of hybrid technology (SPECT/CT and PET/CT) [18, 19]. Nevertheless, obtaining reliable dose estimates after administration of large ^{131}I activity remains challenging due to high radiation flux and count loss. Alternatively, quantitative imaging of iodine tracer was vastly utilized for dose estimation prior to therapy. However, there is a lack of understanding of the consistency between the dose measures from the tracer and those actually received after therapy in addition to the vulnerability of ^{131}I bio-kinetics to change owing to the so-called 'stunning effect' [20, 21].

In light of that, the current study aimed to verify the absorbed doses to salivary glands and pathologic lesions after radioiodine therapy using patients' SPECT/CT scans and earlier phantom investigations in an attempt to resolve dosimetry degrading factors practically.

2 Materials and methods

2.1 Calibration experiment

Acrylic glass body phantom (PET Phantom NEMA 2012 / IEC 2008) was used for the system calibration. A total of 1983.2 MBq ^{131}I was injected into the whole phantom. Thereafter, 20 SPECT/CT scans (≈ 2 scans/ week) were subsequently acquired with Symbia™ T scanner (SIEMENS) until the activity decayed to a neglected counts loss [< 30 MBq]. The acquisition settings were selected as step and shoot mood, 64 projections/π, 25 s/projection, 15% photo-peak window at 364 keV with ± 7% scatter windows, and 128 × 128 matrix size. OSEM algorithm was used for image reconstruction with 8 subsets and different numbers of iterations (10, 20, 30, and 40), followed by low pass Gaussian filtering-9 mm. Regions of interest (ROIs) were drawn over the phantom, middle cylinder, and the whole frame. The counts/activity conversion factor was generated based on the CT scan and 30% is-contour. For count loss correction, a correction factor was derived from the ratio between the measured and true counts of the phantom for every single SPECT/CT scan. Then, a set of mathematical equations were derived for count loss correction to be applied on the patients scans [22].

For partial volume effect correction (PVC), the spheres of 26 cm^3, 11.5 cm^3, 5.6 cm^3, 2.6 cm^3, and 0.5 cm^3 volume were filled with 4:1 activity to background ratio at neglected dead time. ROIs were delineated manually on the CT images and also automatic 30%-isocontour for different quantification methods. Afterward, the measured activity was divided by the true activity mount for obtaining recovery coefficients (RCs) to be later used in lesions dose estimation.

2.2 Counts loss correction

As expected, the measured counts increased non-linearly with larger ^{131}I activity due to machine dead time. Accordingly, a set of bi-compartmental equations combining the whole frame counts and the correction factors were generated for counts loss correction, as follows:

- whole frame counts ≥ 47 kcps,

$$Y = 0.0009X^3 - 0.1039X^2 + 3.9189X - 13.309 \quad R - \text{squared} = 0.98 \tag{1}$$

-whole frame counts ≤ 47 kcps,

$$Y = 5670.9X^{-1.33} \quad R - \text{squared} = 0.93 \tag{2}$$

y: correction factor, X: whole frame counts (kcps).

At neglected dead time, two conversion factors (counts/MBq) were generated; the first was CT- based, and the latter was based on automated iso-thresholding over SPECT images. The CT-based conversion factor was slightly higher than 30% iso-contour in order of 4% at $10_{it.} \times 8_{subsets}$, and 1% at $40_{it.} \times 8_{subsets}$.

2.3 Partial volume effect (PVE)

Recovery coefficients (RCs) were generated from the phantom study to account for the activity underestimation in small objects. The obtained RCs were varied according to the measured volumes from CT and 30%-isocontour methods as demonstarted in Fig. 1. The impact of increasing iterations numbers on the quantification accuracy was shown in Fig. 2. It was revealed that the recovery coefficients improved relatively with larger iterations. Thus, the SPECT/CT scans reconstruction was made by $40_{it.} \times 8_{sub}$ and 9-mm Gaussian filtering for all patients. And the numerical functions shown below were used;

for PVE correction in salivary glands:

$$RC = 0.1726\ln(v) + 0.3208 \quad R - \text{squared} = 0.97 \tag{3}$$

for PVE correction in thyroid residues and lesions:

$$RC = 0.5583 \times v^{0.0989} \quad R - \text{squared} = 0.96 \tag{4}$$

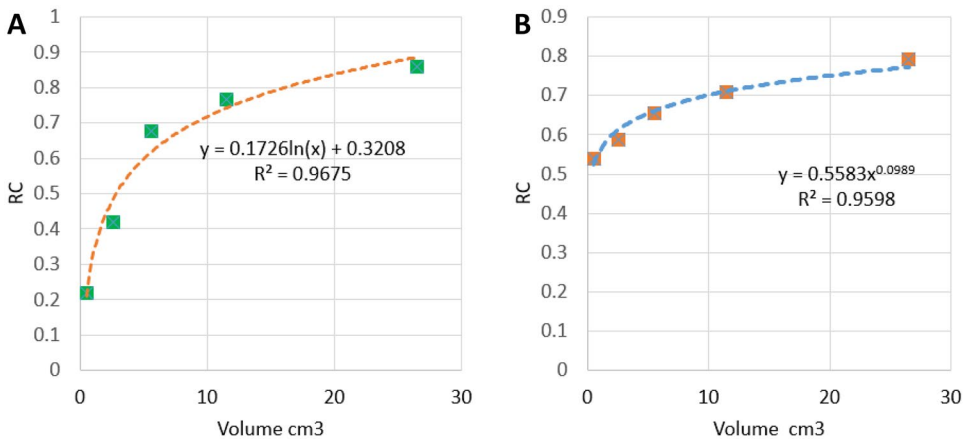

Fig. 1 Volumes versus recovery coefficients from CT scans (**A**) and 30% iso-threshold (**B**) with 40 iterations and 8 subsets

RC: recovery coefficient, v: volume (cm^3).

The real volumes of the spheres were well-correlated with those estimated by both CT and 30%-iso contour, as illustrated in Fig. 3. Accordingly, 30% iso-thresholding was employed to measure the volume and counts of thyroid remnants and distal lesions in the patients' study.

2.4 Clinical study

25 DTC patients (n = 25; 6 males and 19 females) undergoing radioiodine therapy were accepted to join this study. Informed consent was received from all the participant patients according to the ethical review board at Cerrahpasa Medical School. The activity to administer was empirically prescribed (by the referring physicians) and broadly variable based on the clinical case. A range of 3497 to 9250 MBq (median: 5550 MBq) was administered to the participant patients. The median weight was 72 kg (range: 45–114 kg) and the median age was 44 years (range: 19–71). Following oral ^{131}I administration, SPECT/CT scans were subsequently acquired at 4 ± 2, 24 ± 2, and 168 ± 3 h with the settings summarized in Table1.

The participant patients were prepared by thyroid hormone withdrawal (≈ 4 weeks) and the TSH level was above 30 mIU/L. The routinely followed protocol implies lemon stimulation and chewing gum to reduce the salivary glands' uptake.

CT images were used to draw ROIs over the salivary glands, while automated 30% iso-contour was found superior for thyroid residues and distant lesions quantification. The partial volume effect (PVE) and counts loss were corrected using the equations derived from the calibration experiment (Eqs. 1–4). The Uptake values (%) of the targets were calculated at the first and second measurements in proportion to the administered activity. The activity in the target organ A_i was estimated at a given time by:

$$A_i = [C \times (1 + CLCF)]/RC \times CF \quad (5)$$

C: scatter corrected counts, CLCF: Counts loss correction factor, RC: Recovery coefficient, CF: calibration factor.

The total number of disintegrations ($\tilde{A}$) in the salivary glands was estimated from the mono-exponential fitting of the time-activity plots, while the trapezoidal rule was used to generate $\tilde{A}$ in the lesions. The time-integrated activity coefficient ($\bar{a}$) was then calculated by:

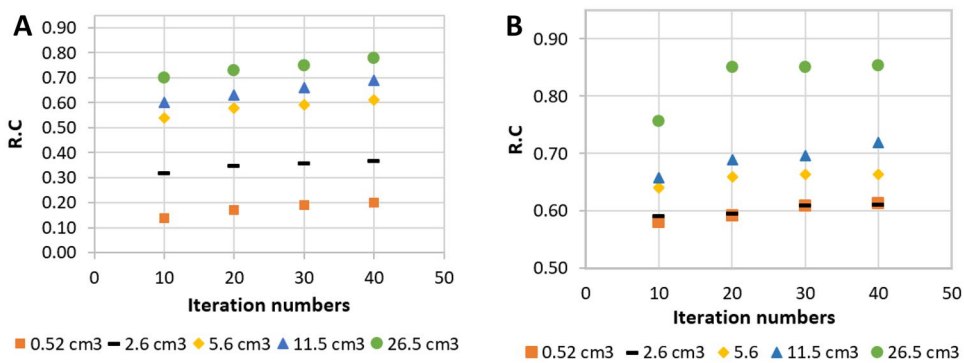

Fig. 2 Recovery coefficients improvement with larger iterations number over **A**) CT scan, and **B**) SPECT with 30%-iso contour

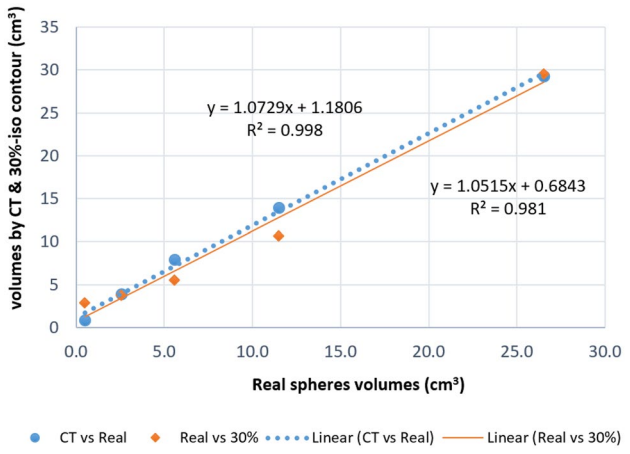

Fig. 3 The consistency between the actual volumes (cm^3) of the spheres and those measured by CT and SPECT with 30%-isocontour

$$\bar{a} = \tilde{A}/A_0 \quad (6)$$

A_o: administered activity, ã: time-integrated activity coefficient (TIAC).

The absorbed dose to salivary glands was calculated by IDAC-Dose 2.1 program. This code is equipped with specific absorbed dose fractions [reported by the International Commission on Radiological Protection (ICRP)] and a computational framework of internal dose assessment given for reference adults in ICRP Publication 133 [23]. However, the absorbed dose to thyroid residues/ lesions was calculated by the unit sphere density model built in the IDAC-Dose 2.1 program. The dose fractions from radioiodine activity for spherical volumes, derived from Monte Carlo simulation methods, have been reported earlier [24].

2.5 Statistical analysis

Mann–Whitney test was used to compare the absorbed doses to submandibular and parotid glands via IBM SPSS Statistics 20.

Table 1 SPECT/CT settings used in the patients' study

Parameter	Type
Scan mood	step and shoot mood
Number of projections	64 projections/π
Projection time	25 s/projection
Matrix size	128 × 128
Scan windows	15% photo-peak window at 364 keV with ± 7% scatter windows
Reconstruction algorithm	OSEM algorithm ($8_{subsets}$ and 40 $_{iterations}$)
Filter	low pass Gaussian filtering-9 mm
Acquisition times	4 ± 2, 24 ± 2, and 168 ± 3 h following treatment

3 Results

3.1 Patients study

The absorbed dose to submandibular glands, parotid glands, thyroid residues, and distal metastases was estimated for 25 patients undergoing radioiodine therapy as reported in table 2. The median volume of the right parotid glands was 26.7 cm^3 (range: 13.0–70.0 cm^3), and 26.2 cm^3 (range: 15.2–62.0 cm^3) for the left parotid glands. The median volumes of the right and left submandibular glands were 12.5 cm^3 (range: 8.00–22.5 cm^3) and 12.0 cm^3 (range: 7.00–21.6 cm^3), respectively. Furthermore, 22 thyroid residues were visualized on SPECT/CT images with a median volume of 5.42 cm^3 (range: 2.82–12.70 cm^3) and 10 pathologic lesions with a median volume of 5.95 cm^3 (range: 2.16–11.50 cm^3). It was difficult to identify such a lesion or thyroid foci in patient number 12 on SPECT/CT.

As summarized in Table 3, the median ^{131}I uptake (%) in the thyroid residues at 4 ± 2 h was 0.82 (range: 0.01–10.9) and gradually increased to 1.20 (range: 0.04–18.3) after 24 ± 2 h. The median uptake in the right parotid glands was 0.18 (range: 0.03–0.57) at 4 ± 2 h and 0.13 (range: 0.002–0.47) at 24 ± 2 h. The median uptake in the left parotid glands was 0.18 (range: 0.02–0.54) at 4 ± 2 h and 0.12 (range: 0.003–0.44) at 24 ± 2 h. Whereas, lower median uptake was manifested in the submandibular glands as 0.10 (range: 0.04–0.21) on the left-sided and 0.07 (range: 0.002–0.15) on the right-sided at 4 ± 2 and 24 ± 2 h, respectively.

Additionally, the interpatient variability in the ^{131}I kinetics was comprehended from the variation in the time-integrated activity coefficients (TAICs). The median TIAC in the left parotid glands was 5.21 min (range: 0.19–25.4) and 4.45 min (range: 0.21–20.4) in the right parotid glands. However, right and left submandibular glands showed lower TIAC values with a median of 2.62 (0.70–8.95) and 2.59 min (range: 1.10–12.2), respectively.

The present work demonstrated that the absorbed dose per unit administered activity to parotid glands varied from 0.04 to 0.97 Gy/GBq with a median of 0.26 Gy/GBq, and the absorbed dose to submandibular glands was lower with a median of 0.14 Gy/GBq ranging from 0.05 to 0.56 Gy/GBq, as illustrated in Fig. 4. A significant difference ($P_{value} < 0.05$) was demonstrated between the absorbed doses to parotid and salivary glands.

On the other hand, the absorbed dose to thyroid remnants varied among the patients as revealed in Table 4. The absorbed dose to thyroid remnants ranged from 0.55 to 399.5 Gy/GBq (median: 21.8 Gy/GBq), and the distal lesions likewise exhibited a broad dose range of 0.78—28.0 Gy/GBq (median: 3.12 Gy/GBq). It was also deduced that only 41% of the thyroid residues received absorbed dose > 80 Gy and 18% between 70–80 Gy following administration of 3497–9250 MBq (median:150 MBq) ^{131}I.

Table 2 The measured volumes (cm^3) of parotid glands and submandibular glands, thyroid residues, and metastases

P.ts	Lt parotid	Rt parotid	Rt submandibular	Lt submandibular	Thyroid residues	Metastases
1	20.1	13.0	12.5	11.3	-	2.16
2	34.3	37.3	22.5	16.9	8.24	-
3	26.2	32.7	9.50	7.70	-	-
4	21.6	26.7	11.9	10.8	12.7	-
5	18.9	17.5	12.0	10.5	3.00	-
6	30.0	24.3	11.4	11.0	3.80	-
7	33.1	34.4	18.5	15.1	4.90	-
8	28.5	15.5	18.0	7.00	6.80	-
9	25.8	25.4	13.2	12.0	5.42	-
10	28.8	29.9	10.0	11.0	5.40	4.80
11	37.0	33.0	16.7	21.6	-	4.60
12	18.8	29.4	15.4	15.7	-	-
13	21.5	27.4	13.1	12.5	6.40	-
14	21.6	22.0	12.0	14.0	4.75	8.32
15	22.4	23.0	14.5	15.2	5.40	-
16	62.0	70.0	15.3	17.7	10.6	7.50
17	18.8	21.5	8.40	10.3	5.34	7.10
18	29.7	21.5	10.6	12.2	6.60	4.90
19	51.0	47.0	8.20	10.4	3.86	-
20	32.7	42.3	14.0	13.0	6.51	-
21	15.2	18.0	10.2	9.10	5.42	-
22	57.0	62.0	16.0	15.0	7.80	4.04
23	26.0	24.0	10.6	10.1	2.82	-
24a	18.0	19.0	17.0	19.0	12.0	11.5
24b	-	-	-	-	-	7.00
25	37.0	35.0	8.0	9.0	6.6	-
Med	**26.2**	**26.7**	**12.5**	**12.0**	**5.42**	**5.95**
Min	**15.2**	**13.0**	**8.00**	**7.00**	**2.82**	**2.16**
Max	**62.0**	**70.0**	**22.5**	**21.6**	**12.7**	**11.5**

Med Median, *Min* Minimum, *Max*. maximum, a: lesion 1, b: lesion 2

Whereas 18% of the patients received doses amidst 40–70 Gy, and the remaining 23% showed absorbed doses less than 40 Gy. In contrast, 18% of the metastases had absorbed doses above 80 Gy, 9% between 40–60 Gy, and the vast majority (64%) exhibited absorbed doses less than 40 Gy.

4 Discussion

Radioiodine therapy is deemed an essential standard of care for DTC with a favorable impact on overall survival [25, 26]. In metastatic DTC patients, the survival rate was significantly decreased and larger activity administration is more demanded [27, 28]. Commonly, a single dose of 7.4 GBq is applied for metastatic DTC, while higher activity (up to 9 GBq) was administered for advanced DTC therapy [27, 28]. In 2015, less intense treatment strategies for many DTC patients including observation or thyroid lobectomy without RIT were recommended by the American Thyroid Association (ATA) making controversial and significant differences in clinical practice [29, 30]. More recently, a joint statement has been released (in 2019) by leading nuclear medicine organizations involving the ATA, European Association of Nuclear Medicine (EANM), Society of Nuclear Medicine and Molecular Imaging (SNMMI), and European Thyroid Association (ETA) that defined the indications and the optimal prescribed activity in RIT by reporting a set of collective principles (Martinique Principles) [31, 32]. Overall, the administered RAI activity can be determined empirically using a "one-dose-fits-all" regime or based on a dosimetric approach. The suggested ^{131}I activities for postoperative ablation/adjuvant RIT were outlined as 1.1–2.2 GBq in low-risk DTC (< 2 cm), 2.2–3.7 GBq in low-risk (> 2 cm), and intermediate-risk DTC, and ≥ 3.7 GBq in high-risk DTC [31]. The empirical approach is simple and effective, however, significant adverse reactions may arise like reduced bone marrow reserve, lung function

Table 3 Uptake values (%) of the submandibular glands, parotid glands, thyroid residues, and metastases

pts	Rt submandibular		Lt submandibular		Lt parotid		Rt parotid		Thyroid residues		Metastases	
	4 ± 2	24 ± 2	4 ± 2	24 ± 2	4 ± 2	24 ± 2	3	24 ± 2	4 ± 2	24 ± 2	4 ± 2	24 ± 2
1	0.15	0.08	0.11	0.06	0.39	0.19	0.28	0.14	-	-	0.03	0.05
2	0.18	0.02	0.2	0.05	0.18	0.13	0.17	0.08	0.8	1.2	-	-
3	0.05	0.03	0.04	0.03	0.09	0.08	0.1	0.07	-	-	-	-
4	0.07	0.05	0.06	0.05	0.1	0.05	0.15	0.08	9.2	16.5	-	-
5	0.09	0.08	0.08	0.07	0.1	0.12	0.08	0.1	9	9.5	-	-
6	0.11	0.05	0.12	0.06	0.42	0.22	0.42	0.14	0.2	1	-	-
7	0.1	0.03	0.08	0.03	0.28	0.12	0.26	0.13	0.5	0.9	-	-
8	0.06	0.08	0.08	0.06	0.15	0.12	0.12	0.13	0.5	1.5	-	-
9	0.08	0.15	0.1	0.17	0.18	0.26	0.15	0.21	2.14	3.2	-	-
10	0.06	0.02	0.06	0.03	0.24	0.21	0.38	0.47	10.5	2.56	0.44	0.67
11	0.14	0.11	0.1	0.09	0.05	0.03	0.04	0.03	-	-	0.01	0.03
12	0.05	0.14	0.05	0.14	0.06	0.24	0.1	0.26	-	-	-	-
13	0.12	0.04	0.04	0.06	0.19	0.04	0.19	0.08	1	0.05	-	-
14	0.1	0.07	0.08	0.06	0.16	0.05	0.11	0.05	5.2	6	0.3	0.5
15	0.06	0.05	0.07	0.04	0.23	0.37	0.21	0.28	0.39	1.2	-	-
16	0.08	0.08	0.08	0.07	0.41	0.36	0.34	0.46	1	1.2	0.18	0.28
17	0.06	0.03	0.06	0.04	0.17	0.32	0.18	0.31	0.01	0.54	0	0.22
18	0.2	0.08	0.27	0.14	0.41	0.08	0.32	0.07	4.36	9.58	1.74	0.82
19	0.04	0.02	0.07	0.03	0.26	0.12	0.19	0.08	10.85	18.27	-	-
20	0.04	0.1	0.07	0.3	0.17	0.2	0.14	0.13	0.07	0.3	-	-
21	0.11	0.11	0.13	0.18	0.14	0.07	0.11	0.07	5.63	9.7	-	-
22	0.14	0.04	0.18	0.11	0.19	0.08	0.23	0.1	0.15	0.24	0.11	0.06
23	0.21	0.1	0.34	0.23	0.54	0.26	0.57	0.29	0.34	0.23	-	-
24a	0.11	0	0.12	0.02	0.02	0	0.03	0	0.06	0.04	0.24	0.1
24b	-	-	-	-	-	-	-	-	-	-	0.03	0.028
25	0.1	0.09	0.12	0.12	0.43	0.44	0.39	0.35	0.75	0.82	-	-
Med	**0.10**	**0.07**	**0.08**	**0.06**	**0.18**	**0.12**	**0.18**	**0.13**	**0.82**	**1.20**	**0.15**	**0.16**
Min	**0.04**	**0.002**	**0.04**	**0.02**	**0.02**	**0.003**	**0.03**	**0.002**	**0.01**	**0.04**	**0.004**	**0.03**
Max	**0.21**	**0.15**	**0.34**	**0.3**	**0.54**	**0.44**	**0.57**	**0.47**	**10.9**	**18.3**	**1.74**	**0.82**

Med median, *Min* minimum, *Max*. maximum, a: lesion 1, b: lesion 2

impairment, and progressive loss of efficacy after repeated treatment [31]. In contrast, the latter dosimetric approach is more complicated and provides patient-tailored activities with several advantages of high success rates in a single treatment, avoiding suboptimal or excessive ^{131}I administration, the possibility to plan the activity to the target volume, and reducing radiation toxicity [31, 33–35]. The integrated CT in hybrid SPECT/CT was a key element for resolving dosimetry problems and improving quantitative accuracy, however, a few inherited uncertainties in dose calculation are still matters of concern [36, 37]. Though it is challenging to confirm a preference between the empiric or dosimetric approach for RIT, the latter strategy may be more effective in subjects with critical conditions (e.g., renal failure, diffuse lung metastases, and reduced bone marrow reserve) [31].

On the other hand, long-term sequelae and elevation of morbidity rates are associated with ^{131}I treatment as well as salivary glands deterioration. Unlike tracer-based dosimetry, this study sought to provide clinically validated method for post-therapeutic dose estimates. From the technical side, the calibration tests with IEC PET phantom and SPECT/CT were made to improve the dose calculation accuracy. The triple energy windows method was utilized for scatter correction with a feasible compromise between accuracy and noise as recommended in past ^{131}I studies [38, 39]. For PVE correction, recovery coefficients were derived to compensate for the activity underestimation in anatomic structures (e.g. salivary glands and lesions) approximated by spherical shape. However, this method might not be a typical model due to interference of other factors such as shape, signal-to-noise ratio, and position in the image. Alternatively, the geometric transfer matrix has been shown effective to improve SPECT quantitative accuracy by using the point spread function to calculate regional contribution fractions [40, 41]. In addition, the accuracy of the area under time-activity curve is associated with several factors

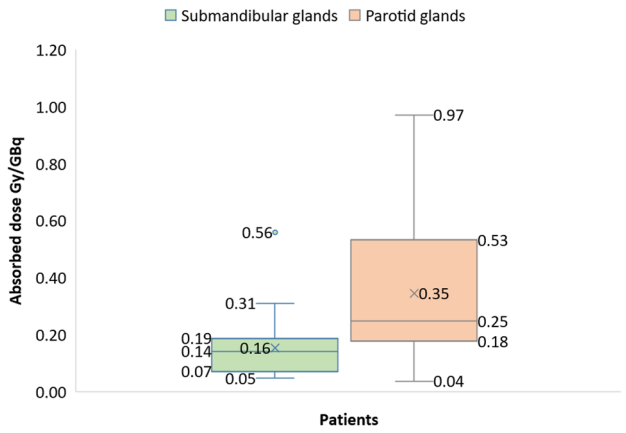

Fig. 4 whisker plot of the absorbed dose values for parotid and submandibular glands

like the number of samples, sampling time, and the fitting function [41]. Unfortunately, it was impossible to increase the number of SPECT/CT acquisitions in this study because of the global covid-19 pandemic.

From the clinical standpoint, earlier salivary glands assessment and follow-up showed a wide absorbed dose range from 0.03 to14 Gy/ GBq [42]. In another report, the absorbed dose range to a single parotid and submandibular gland was found 0.10–0.30 Gy/GBq and 0.20–1.20 Gy/GBq, respectively [43]. However, these studies like others were based on serial planar images with several estimation errors related to volume determination, background ROIs, and scatter contribution. Exceptionally, Jentzen and co-authors estimated the absorbed dose to submandibular glands (0.35 ± 0.14 Gy/GBq) and parotid glands (0.33 ± 0.09 Gy/GBq) using ^{124}I PET/CT under lemon-juice stimulation [44]. In contrast, the current study demonstrated that the absorbed dose per unit administered activity to parotid glands varied from 0.04 to 0.97 Gy/GBq with a median of 0.26 Gy/GBq. Whereas, the median dose to submandibular glands was 0.14 Gy/GBq ranging from 0.05 to 0.56 Gy/GBq. The agreement between the current findings obtained after ^{131}I therapy and the aforementioned ^{124}I PET/CT study ascertain the accuracy of the implemented method for post-therapeutic dose estimation.

Clinically, the computed absorbed doses per administered activity are indeed small to cause significant damage to salivary glands. However, the oversensitivity to low radiation levels is attributed to the unique combination of mucous and serous acinar cells in the salivary glands [42]. In radiotherapy, a complete loss of salivary glands function has been shown at 60 Gy. However, the dysfunction of salivary glands occurs in a dose-dependent manner after radioiodine therapy [42, 44]. For example, a single dose of 6 GBq resulted in a partial function loss of 30%, while cumulative administration of 35 GBq caused a complete glandular failure [42]. Moreover, mild dysfunction was observed in 60% of patients following

Table 4 Absorbed dose (Gy/GBq) to thyroid residues and metastases

Patients	Thyroid residues	Metastases
1	-	3.0
2	15.6	-
3	-	-
4	153.5	-
5	399.5	-
6	25.6	-
7	20.4	-
8	21.8	-
9	61.2	-
10	76.5	14.8
11	-	0.8
12	-	-
13	3.10	-
14	153.0	7.6
15	22.9	-
16	13.2	4.3
17	11.1	3.3
18	199.0	28
19	303.4	-
20	3.20	-
21	193.0	-
22	3.80	1.9
23	11.1	-
24a	0.55	1.8
24b	-	0.8
25	15.2	-
Median	**21.8**	**3.12**
Minimum	**0.55**	**0.78**
Maximum	**399.5**	**28.0**

RIT with 5143–5550 MBq including decreased uptake and delayed excretion in parotid glands. A similar degree of dysfunction was also manifested in the submandibular glands for 45% of patients. In addition, moderate to severe dysfunction and decreased uptake were noted with more iodine therapies [45–47]. It has been recently supported that the mean parotid dose should be kept below 26 Gy for the preservation of salivary gland function in radiotherapy and a mean dose < 20 Gy might increase the local recurrence risk for head and neck cancer [48]. On the basis of our findings, a cumulative activity of 27 GBq is probably adequate to deliver the preservation dose (26 Gy) of the parotid gland, and 46 GBq is expected to induce parotid glands failure according to the parotid glands dose of 0.97 Gy/GBq and maximum tolerated dose of 45 Gy.

In lesion dosimetry, the present work exhibited notably disparate dose values for thyroid remnants (range: 0.5–399.5 Gy/GBq) and metastases (range: 0.78–15 Gy/GBq). In contrast, previous ^{131}I tracer-based data demonstrated variable absorbed doses to thyroid remnants and metastases ranging from 5 to 1000 Gy

[49–51]. This consistency represents further proof of the accuracy of the dosimetry method used here.

Moreover, it was revealed that only 41% of the thyroid residues received an absorbed dose > 80 Gy, 18% had an absorbed dose between 70–80 Gy, 18% were with a dose range of 40–70 Gy, and 23% received absorbed dose below 40 Gy following administration of 5402 ± 1665 MBq ^{131}I. Whereas, 18% of the distal lesions exhibited absorbed doses above 80 Gy and 9% between 40–60 Gy, while the vast majority of lesions (73%) received doses less than 40 Gy. In dosimetry-oriented therapy, thyroid ablation was successfully achieved with absorbed doses > 49 Gy, 90 Gy, and 300 Gy, while partial to complete response was reported for distal metastases after receiving doses higher than 40 Gy to 80 Gy [17, 51].

Herein, the safety and efficacy of ^{131}I therapy are exquisitely favorable outcomes for DTC patients that must be achieved with personalized data and well-validated dosimetry methods. Prospectively, this method might be feasibly used for establishing a dose–effect relationship relying on reliable dose estimates after RI therapy.

5 Conclusion

Dose estimation to salivary glands and pathologic lesions, identified by SPECT/CT, has been shown to be feasible following RIT, together with good agreement with ^{131}I-tracer and ^{124}I-PET/CT-based studies. A significant salivary glands uptake has been shown in the early hours that may affect the accuracy of the measured thyroid uptake by the standard probe. A broad and sub-effective dose range was estimated for thyroid residues and distal lesions. The feasibility of the current dosimetry method may be useful to establish a dose–effect relationship in RIT based on post-therapeutic dose estimates.

Acknowledgements The authors express sincere thanks to the team of SPECT/CT at Cerrahpaşa Medical School.

Declarations

Ethical approval Institutional Review Board approval was obtained according to the decision number 29281604–604.01.01–2226.

Informed consent Written informed consent was obtained from all subjects (patients) in this study.

Conflict of interest The authors of this manuscript declare no relationships with any companies whose products or services may be related to the article's subject matter.

References

1. Fugazzola L, Elisei R, Fuhrer D, et al. European Thyroid Association Guidelines for the Treatment and Follow-Up of Advanced Radioiodine-Refractory Thyroid Cancer. Eur Thyroid J. 2019;8(5):227–45. https://doi.org/10.1159/000502229.
2. Cayir D, Mine A. Radioiodine Therapy of Malignant Thyroid Diseases. Radionuclide Treatments. 2017;21.
3. Schmidbauer B, Menhart K, Hellwig D, Grosse J. Differentiated Thyroid Cancer-Treatment: State of the Art. Int J Mol Sci. 2017;18(6):1292. Published 2017 Jun 1. https://doi.org/10.3390/ijms18061292.
4. Wyszomirska A. Iodine-131 for therapy of thyroid diseases. Physical and biological basis. Nucl Med Rev Cent East Eur. 2012;15(2):120–123. Published 2012 Aug 28.
5. Verburg FA, Giovanella L, Iakovou I, Konijnenberg MW, Langsteger W, Lassmann M, Mihailovic J, Luster M. I-131 as adjuvant treatment for differentiated thyroid carcinoma may cause an increase in the incidence of secondary haematological malignhematologicalconvenient" truth? Eur J Nucl Med Mol Imaging. 2018;45(13):2247–9. https://doi.org/10.1007/s00259-018-4184-z. Epub 2018 Oct 8 PMID: 30298378.
6. Lin JD, Kuo SF, Huang BY, Lin SF, Chen ST. The efficacy of radioactive iodine for the treatment of well-differentiated thyroid cancer with distant metastasis. Nucl Med Commun. 2018;39(12):1091–6. https://doi.org/10.1097/MNM.0000000000000897.
7. Krishnamurthy S, Vasudeva SB, Vijayasarathy S. Salivary gland disorders: A comprehensive review. World J Stomatol. 2015;4(2):56–71.
8. Riachy R, Ghazal N, Haidar MB, Elamine A, Nasrallah MP. Early Sialadenitis After Radioactive Iodine Therapy for Differentiated Thyroid Cancer: Prevalence and Predictors. Int J Endocrinol. 2020;2020:8649794. Published 2020 Aug 4. https://doi.org/10.1155/2020/8649794
9. Bhayani MK, Acharya V, Kongkiatkamon S, et al. Sialendoscopy for Patients with Radioiodine-Induced Sialadenitis and Xerostomia. Thyroid. 2015;25(7):834–8. https://doi.org/10.1089/thy.2014.0572.
10. Chow SM. Side effects of high-dose radioactive iodine for ablation or treatment of differentiated thyroid carcinoma. J Hong Kong College Radiol. 2005;8(3):127.
11. Kita T, Yokoyama K, Higuchi T, et al. Multifactorial analysis on the short-term side effects occurring within 96 hours after radioiodine-131 therapy for differentiated thyroid carcinoma. Ann Nucl Med. 2004;18(4):345–9. https://doi.org/10.1007/BF02984474.
12. Walter MA, Turtschi CP, Schindler C, Minnig P, Müller-Brand J, Müller B. The dental safety profile of high-dose radioiodine therapy for thyroid cancer: long-term results of a longitudinal cohort study. J Nucl Med. 2007;48(10):1620–5. https://doi.org/10.2967/jnumed.107.042192. Epub 2007 Sep 14 PMID: 17873131.
13. Jonklaas J, Wang H, Esposito G. Salivary Function after Radioiodine Therapy: Poor Correlation between Symptoms and Salivary Scintigraphy. Front Endocrinol (Lausanne). 2015;6:100. Published 2015 Jun 17. https://doi.org/10.3389/fendo.2015.00100
14. Jeong SY, Kim HW, Lee SW, Ahn BC, Lee J. Salivary gland function 5 years after radioactive iodine ablation in patients with differentiated thyroid cancer: direct comparison of pre- and postablation scintigraphies and their relation to xerostomia symptoms. Thyroid. 2013;23(5):609–16. https://doi.org/10.1089/thy.2012.0106.
15. Kabasakal L, AbuQbeitah M, Aygün A, et al. Pre-therapeutic dosimetry of normal organs and tissues of (177) Lu-PSMA-617 prostate-specific membrane antigen (PSMA) inhibitor in patients with castration-resistant prostate cancer. Eur J Nucl Med Mol Imaging. 2015;42(13):1976–83. https://doi.org/10.1007/s00259-015-3125-3.
16. Wang XY, Yu J, Zhang FY, Liu KJ, Xiang B. Phenylephrine Alleviates ^{131}I Radiation Damage in Submandibular Gland Through Maintaining Mitochondrial Homeostasis. Int J Radiat Oncol Biol Phys. 2019;104(3):644–55. https://doi.org/10.1016/j.ijrobp.2019.02.048.
17. Flux GD, Haq M, Chittenden SJ, et al. A dose-effect correlation for radioiodine ablation in differentiated thyroid cancer. Eur J Nucl Med Mol Imaging. 2010;37(2):270–5. https://doi.org/10.1007/s00259-009-1261-3.
18. Peters SMB, van der Werf NR, Segbers M, et al. Towards standardization of absolute SPECT/CT quantification: a multi-center and

multi-vendor phantom study. EJNMMI Phys. 2019;6(1):29. Published 2019 Dec 26. https://doi.org/10.1186/s40658-019-0268-5
19. Bailey DL, Willowson KP. Quantitative SPECT/CT: SPECT joins PET as a quantitative imaging modality. Eur J Nucl Med Mol Imaging. 2014;41(Suppl 1):S17–25. https://doi.org/10.1007/s00259-013-2542-4.
20. Lassmann M, Luster M, Hänscheid H, Reiners C. Impact of 131I diagnostic activities on the biokinetics of thyroid remnants. J Nucl Med. 2004;45(4):619–25.
21. McDougall IR, Iagaru A. Thyroid stunning: fact or fiction? Semin Nucl Med. 2011;41(2):105–12. https://doi.org/10.1053/j.semnuclmed.2010.10.004.
22. Dewaraja YK, Frey EC, Sgouros G, Brill AB, Roberson P, Zanzonico PB, Ljungberg M. MIRD pamphlet No. 23: quantitative SPECT for patient-specific 3-dimensional dosimetry in internal radionuclide therapy. J Nucl Med. 2012;53(8):1310–25. https://doi.org/10.2967/jnumed.111.100123. Epub 2012 Jun 28. PMID: 22743252; PMCID: PMC3465844.
23. Andersson M, Johansson L, Eckerman K, Mattsson S. IDAC-Dose 2.1, an internal dosimetry program for diagnostic nuclear medicine based on the ICRP adult reference voxel phantoms. EJNMMI Res. 2017;7(1):88. Published 2017 Nov 3. https://doi.org/10.1186/s13550-017-0339-3
24. Abuqbeitah M, Sağer S, Demir M, Yeyin N, Akovalı B, Sönmezoğlu K. The impact of different computational assumptions in ^{131} I dosimetry for hyperthyroidism therapy. Med Phys. 2020;47(11):5810–6. https://doi.org/10.1002/mp.14478.
25. Flux GD, Sjogreen Gleisner K, Chiesa C, et al. From fixed activities to personalized treatments in radionuclide therapy: lost in translation? Eur J Nucl Med Mol Imaging. 2018;45(1):152–4. https://doi.org/10.1007/s00259-017-3859-1.
26. Council of the European Union. European Council Directive 2013/59/Euratom on basic safety standards for protection against the dangers arising from exposure to ionising radiation and repealing Directives 89/618/Euratom, 90/641/Euratom, 96/29/Euratom, 97/43/Euratom and 2003/122/Euratom. Official J Eur Union.
27. Abuqbeitah M, Demir M, Kabasakal L, et al. Indirect assessment of the maximum empirical activity (250 mCi) with respect to dosimetry concepts in radioiodine therapy of metastatic differentiated thyroid cancer. Nucl Med Commun. 2018;39(11):969–75. https://doi.org/10.1097/MNM.0000000000000900.
28. Haq MS, McCready RV, Harmer CL. Treatment of advanced differentiated thyroid carcinoma with high activity radioiodine therapy. Nucl Med Commun. 2004;25(8):799–805. https://doi.org/10.1097/01.mnm.0000136693.94761.5c.
29. Haugen BR, Alexander EK, Bible KC, Doherty GM, Mandel SJ, Nikiforov YE, Pacini F, Randolph GW, Sawka AM, Schlumberger M, Schuff KG, Sherman SI, Sosa JA, Steward DL, Tuttle RM, Wartofsky L. 2015 American Thyroid Association Management Guidelines for Adult Patients with Thyroid Nodules and Differentiated Thyroid Cancer: The American Thyroid Association Guidelines Task Force on Thyroid Nodules and Differentiated Thyroid Cancer. Thyroid. 2016;26(1):1–133. https://doi.org/10.1089/thy.2015.0020.PMID:26462967;PMCID:PMC4739132.
30. Luster M, Clarke SE, Dietlein M, Lassmann M, Lind P, Oyen WJ, Tennvall J, Bombardieri E; European Association of Nuclear Medicine (EANM). Guidelines for radioiodine therapy of differentiated thyroid cancer. Eur J Nucl Med Mol Imaging. 2008;35(10):1941–59. https://doi.org/10.1007/s00259-008-0883-1. PMID: 18670773.
31. Campennì A, Barbaro D, Guzzo M, Capoccetti F, Giovanella L. Personalized management of differentiated thyroid cancer in real life - practical guidance from a multidisciplinary panel of experts. Endocrine. 2020;70(2):280–291. https://doi.org/10.1007/s12020-020-02418-x. Epub 2020 Aug 9. PMID: 32772339; PMCID: PMC7581611.
32. Tuttle RM, Ahuja S, Avram AM, Bernet VJ, Bourguet P, Daniels GH, Dillehay G, Draganescu C, Flux G, Führer D, Giovanella L, Greenspan B, Luster M, Muylle K, Smit JWA, Van Nostrand D, Verburg FA, Hegedüs L. Controversies, Consensus, and Collaboration in the Use of ^{131}I Therapy in Differentiated Thyroid Cancer: A Joint Statement from the American Thyroid Association, the European Association of Nuclear Medicine, the Society of Nuclear Medicine and Molecular Imaging, and the European Thyroid Association. Thyroid. 2019;29(4):461–70. https://doi.org/10.1089/thy.2018.0597. PMID: 30900516.
33. Brans B, Bodei L, Giammarile F, et al. Clinical radionuclide therapy dosimetry: the quest for the "Holy Gray." Eur J Nucl Med Mol Imaging. 2007;34(5):772–86. https://doi.org/10.1007/s00259-006-0338-5.
34. Garin E, Boucher E, Rolland Y. 99mTc-MAA-based dosimetry for liver cancer treated using 90Y-loaded microspheres: known proof of effectiveness. J Nucl Med. 2014;55(8):1391–2. https://doi.org/10.2967/jnumed.114.137422.
35. Lee JJ, Chung JK, Kim SE, et al. Maximal safe dose of I-131 after failure of standard fixed dose therapy in patients with differentiated thyroid carcinoma. Ann Nucl Med. 2008;22(9):727–34. https://doi.org/10.1007/s12149-007-0179-8.
36. Kletting P, Schimmel S, Kestler HA, et al. Molecular radiotherapy: the NUKFIT software for calculating the time-integrated activity coefficient [published correction appears in Med Phys. 2014 Mar;41(3):037201] [published correction appears in Med Phys. 2014 Mar;41(3):]. Med Phys. 2013;40(10):102504. https://doi.org/10.1118/1.4820367
37. Gear JI, Cox MG, Gustafsson J, et al. EANM practical guidance on uncertainty analysis for molecular radiotherapy absorbed dose calculations. Eur J Nucl Med Mol Imaging. 2018;45(13):2456–74. https://doi.org/10.1007/s00259-018-4136-7.
38. Dewaraja YK, Koral KF, Fessler JA. Regularized reconstruction in quantitative SPECT using CT side information from hybrid imaging. Phys Med Biol. 2010;55(9):2523–39. https://doi.org/10.1088/0031-9155/55/9/007.
39. Buckley SE, Saran FH, Gaze MN, et al. Dosimetry for fractionated (131)I-mIBG therapies in patients with primary resistant high-risk neuroblastoma: preliminary results. Cancer Biother Radiopharm. 2007;22(1):105–12. https://doi.org/10.1089/cbr.2007.301.
40. Thomas BA, Cuplov V, Bousse A, et al. PETPVC: a toolbox for performing partial volume correction techniques in positron emission tomography. Phys Med Biol. 2016;61(22):7975–93. https://doi.org/10.1088/0031-9155/61/22/7975.
41. Dewaraja YK, Ljungberg M, Green AJ, et al. MIRD pamphlet No. 24: Guidelines for quantitative 131I SPECT in dosimetry applications. J Nucl Med. 2013;54(12):2182–2188. https://doi.org/10.2967/jnumed.113.122390
42. Nabaa B, Takahashi K, Sasaki T, Okizaki A, Aburano T. Assessment of salivary gland dysfunction after radioiodine therapy for thyroid carcinoma using non-contrast-enhanced CT: the significance of changes in volume and attenuation of the glands. AJNR Am J Neuroradiol. 2012;33(10):1964–70. https://doi.org/10.3174/ajnr.A3063.
43. Jentzen W, Schneider E, Freudenberg L, et al. Relationship between cumulative radiation dose and salivary gland uptake associated with radioiodine therapy of thyroid cancer. Nucl Med Commun. 2006;27(8):669–76. https://doi.org/10.1097/00006231-200608000-00009.
44. Jentzen W, Richter M, Nagarajah J, et al. Chewing-gum stimulation did not reduce the absorbed dose to salivary glands during radioiodine treatment of thyroid cancer as inferred from pre-therapy (124)I PET/CT imaging. EJNMMI Phys. 2014;1(1):100. https://doi.org/10.1186/s40658-014-0100-1.
45. Solans R, Bosch JA, Galofré P, et al. Salivary and lacrimal gland dysfunction (sicca syndrome) after radioiodine therapy. J Nucl Med. 2001;42(5):738–43.
46. Wang ZH, Yan C, Zhang ZY, et al. Radiation-induced volume changes in parotid and submandibular glands in patients with head and neck cancer receiving postoperative radiotherapy: a longitudinal study. Laryngoscope. 2009;119(10):1966–74. https://doi.org/10.1002/lary.20601.

47. Barker JL Jr, Garden AS, Ang KK, et al. Quantification of volumetric and geometric changes occurring during fractionated radiotherapy for head-and-neck cancer using an integrated CT/linear accelerator system. Int J Radiat Oncol Biol Phys. 2004;59(4):960–70. https://doi.org/10.1016/j.ijrobp.2003.12.024.
48. Wu VWC, Leung KY. A Review on the Assessment of Radiation Induced Salivary Gland Damage After Radiotherapy. Front Oncol. 2019;9:1090. Published 2019 Oct 17. https://doi.org/10.3389/fonc.2019.01090
49. Maxon HR, Thomas SR, Hertzberg VS, et al. Relation between effective radiation dose and outcome of radioiodine therapy for thyroid cancer. N Engl J Med. 1983;309(16):937–41. https://doi.org/10.1056/NEJM198310203091601.
50. Wierts R, Brans B, Havekes B, et al. Dose-Response Relationship in Differentiated Thyroid Cancer Patients Undergoing Radioiodine Treatment Assessed by Means of 124I PET/CT. J Nucl Med. 2016;57(7):1027–32. https://doi.org/10.2967/jnumed.115.168799.
51. Stokke C, Gabiña PM, Solný P, et al. Dosimetry-based treatment planning for molecular radiotherapy: a summary of the 2017 report from the Internal Dosimetry Task Force. EJNMMI Phys. 2017;4(1):27. Published 2017 Nov 21. https://doi.org/10.1186/s40658-017-0194-3